Experimental study of large scale plunging jets

Grégory Guyot, Mathieu Rodriguez, Michael Pfister, Jean-Philippe Matas, Alain H. Cartellier

6th International Symposium on Hydraulic Structures Portland, Oregon, USA, 27-30 June 2016
Hydraulic Structures and Water System Management
DOI: UUUUUUUUUU

Experimental study of large scale plunging jets

G. GUYOT[1,5], M. RODRIGUEZ[2], M. PFISTER[3], J.P. MATAS[4] and A. CARTELLIER[5]
[1]EDF Hydraulic Engineering Center
Savoie Technolac, 73370 Le Bourget du lac, France
[2]CERG Lab
7, rue Lavoisier, 38800 Le Pont de Claix, France
[3] Laboratory of Hydraulic Constructions (LCH)
EPFL
Station 8, 1015, Lausanne, Suisse
[4]LMFA - Université Claude Bernard Lyon I
43, boulevard du 11 novembre 69 622 Villeurbanne Cedex, France
[5] Université Grenoble Alpes, CNRS, LEGI, F-38000 Grenoble, France
E-mail: gregory.guyot@edf.fr

ABSTRACT

The lack of knowledge regarding the air entrainment caused by large jets in hydraulic structures, especially downstream Pelton turbines, has led EDF (Electricité de France) to carry out a dedicated experiment to the enhancement of the La Coche Power plant. The data extracted from this work have been used to provide a more precise analyze to follow a research purpose.

The first part of this study, is detailed in this article, it has been confirmed that physical phenomena concerning the behavior of large scale plunging jets are still not well understood. The available data measured downstream the jet impact with the first experimental apparatus have been analyzed and compared to data from the literature. The main parameters which have been studied are: the penetration depth, the entrained air flow rate, the average bubble size under the free surface and the accent slope of the bubble plume bottom. Globally the different relations are not scalable with jet scale. Moreover it appeared that the variables are intimately linked to the jet state upstream the impact point. Consequently a second experimental set was designed to measure the dynamic pressure and the void rate inside the jet. The experimental results have shown that a quite simple parameter as the breaking length is not well forecasted by existing formula. The high frequency videos have proven in certain cases that a jet is still continuous when the main formulae predict a broken jet. In addition to that, the experimentations show that the jets are flapping during the fall what is too difficult to understand with the classical way of investigations (pressure sensor and optical probe) which are not synchronized with the jet motion.

Keywords: *Plunging jet, air entrainment, experimental jet statement.*

1. INTRODUCTION

Air-entrainment flows caused by a transition between free-surface flows and confined flows are often involved in hydro-power projects. In the available literature regarding the air entrainment due to a plunging jet, only five references are close to the hydro-power structures scales concerning the jet diameters range. The following references have been found: Donk (1981), Falvey and al.(1987),Evans and al.(1992), Ervine and al.(1997), Duarte, (2014). When considering the same range of falling height, only the four followings references are close the targetted conditions, namelly Elsawy and al.(1980), McKeogh and al.(1981), Falvey H. and al.(1987), Ervine and al.(1997). If both of the jet diameter and the fall height are , only the studies : Falvey. and al. (1987) and Ervine and al.(1997) happen to be close to the present configurations. An improved knowledge of the air-disturbed flows would obviously enable to increase the efficiency of the design studies which tackle the feasibility or the cost of projects. The main application fields are the jet impact in a downstream basin of a Pelton turbine or the jet impact on a concrete structure. Hence, an experimentation dedicated to the "La Coche Pelton" hydraulic power-plant enhancement (EDF France) is valuable to fairly define the air flow rate entrained by the vertical jet, the bubbles size, the penetration depth in the downstream flow. Nowadays two jet powers have been observed with five different discharges with two large scale lab experiments. Around 800 points have been garnered for the downstream flow and around 220 points have been already measured in the plunging jet. The purpose is to

understand the mechanisms which cause the air entrainment downstream the impact, and the bubble cloud behavior in the downstream flow. This article tackles the first step of the experimental study. Firstly the experimental apparatus and the jet configurations will be detailed. Then the key variables in the bubble plume will be discussed. The results of this work lead to refine our understanding of the jet state before the impact point. For this reason, the void fraction and the pressure measurement and the calculation of the break-up length will be also mentioned in the last part of this work.

2. EXPERIMENTAL APPARATUS

Two experimental apparatuses were used to evaluate the jets impact and the behavior of the air entrained under the free surface. The first one was erected on the Pont de Claix channel (EDF France) (Figure 2). This first experimental stand aimed at analyzing the behavior of the air entrained by the jet under the free surface in the downstream channel. The second one was erected in the CERG (Centre d'Etude et de Recherche de Grenoble) (Grenoble France) to provide data regarding the jet structure before its impact.

2.1. General jet configurations

Nozzle diameter (D_0)(mm)	135	135	164	164	164
Jet Flow rate (Q)(L/s)	80	110	50	80	110
Nozzle outlet velocity (V_0) (m/s)	5.59	7.68	2.37	3.79	4.73
Nozzle outlet Reynolds number (Re)	754512	1037454	388183	621092	776366
Nozzle outlet Froude number (Fr)	4.86	6.68	1.87	2.99	3.73
Nozzle outlet Weber number (We)	57766	109215	12587	32221	50346

Table 1: The five studied jets configuration

$\mathrm{Re} = \rho_l V_0 D_0 / \mu$ *(1): Reynolds number;* $Fr = V_0 / \sqrt{gD_0}$ *(2): Froude number,* $We = \rho_l V_0^2 D_0 / \sigma$ *(3): Weber number*

Where g is gravity acceleration, V_0 is the average velocity at the nozzle outlet, D_0 is the nozzle diameter μ is the liquid dynamic viscosity, ρ_l is the volumetric mass density of the liquid, σ is surface tension. all in SI units.

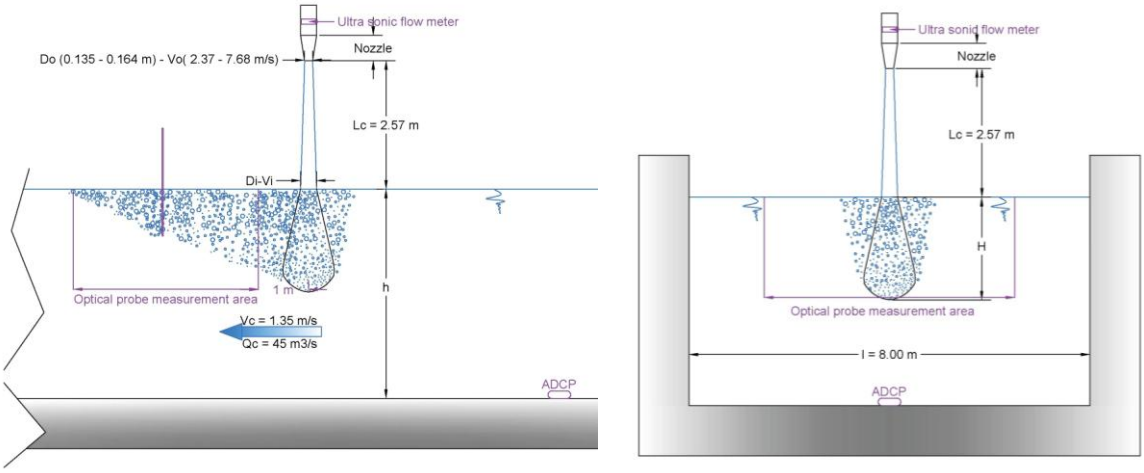

(a) (b)

Figure 1: Longitudinal scheme of the Channel experimental apparatus (a), Elevation scheme (b).

The Reynolds numbers indicate that the flow is fully turbulent at the nozzle outlet, whereas the Weber numbers show that the inertia largely dominate the effect of surface tension.

In the available literature on air entrainment due to a plunging jet, only five references with the same range of jet diameters have been found: Donk (1981), Falvey and al.(1987),Evans and al.(1992), Ervine et al.(1997), Duarte, (2014),. When considering the same range of falling height, only the four followings references are close to our conditions, namelly Elsawy and al.(1980), McKeogh and al. (1981), Falvey and al.(1987), Ervine and al. (1997). With respect to both the jet diameter and the fall height, only the studies Falvey and al.(1987) and Ervine and al.(1997) happen to be close to the present configurations.

2.2. Channel experimental apparatus

(a) (b) (c)

Figure 2: View of the: channel upstream part (a), experimental platform (b), downstream part of the channel(c).

The experimental apparatus was located 300 m downstream the inlet weir of the strictly straight channel and 500 m upstream the channel end. The channel is a 8 meters wide (l) and 5 meters high rectangular waterway. The water level in the channel was controlled by an inlet weir. The channel flow rate (Q_c) was imposed by a hydro power plant downstream. The available range of channel flow rates was 35-80 m^3s^{-1}. For practical reasons, the channel flow rate (Q_c) was set to 45 m^3s^{-1}. Thus, the average channel velocity (V_c) under the jet was 1.35 ms^{-1} (Figure 2). The flow height (h) of the channel was set to ensure a 2.57 meters falling height (L_c) between the jet nozzle and the free water surface (Figure 1).
The jet flow rate (Q) was pumped in the channel upstream the experimental platform by two pumps which fed the PVC 164.3 mm internal diameter circular pipe network. The outlet of this network was the injector itself (Figure 3) which comprised a divergent (I.D. 164 mm to 320 mm) linked to a 600 mm of 320 mm I.D. pipe. A 90° Elbow links the inlet network with the injector. Two calming trash racks were located in the straight part to decrease the turbulence level before the nozzle inlet. The two nozzles, presented in
Figure 3, are conical with the same convergent 0.32 (H/V) slope (Figure 3). The nozzle outlet internal diameters (D_0) are 164 mm and 135 mm with a respective length of 500 mm and 592 mm. Consequently the jet falls down in an atmospheric surrounding. The jet flow rate was imposed by a dimmer switch which drove the pumps. A Krohne Optisonic ultrasonic flow meter located upstream the injector enabled to measure the flow rate.

All the results regarding air entrainment were obtained with an RBI optical probe. This probe was attached to a mast which was able to move in the three directions: X upstream-downstream (from 1 m downstream the jet to the end of the bubble cloud), Y left bank- right bank (between -2.5 m to 2.5m centered on the jet) and Z water depth (up 2 m penetration depth H), as shown in Figure 1 and Figure 3. For each jet configuration, that probe was used to provide the void rate, the bubble size distribution, the air flow rate, the penetration depth and the bubble plume shape along three channel sections downstream the jet. The first one was located 1 m downstream the jet, the second one took place at the middle of the white water induced by the jet and the last was located of around 30 cm before the disappearance of the surface white water.

$$\alpha = \frac{\sum Tg}{Tt} \qquad \textit{(4): Void fraction definition}$$

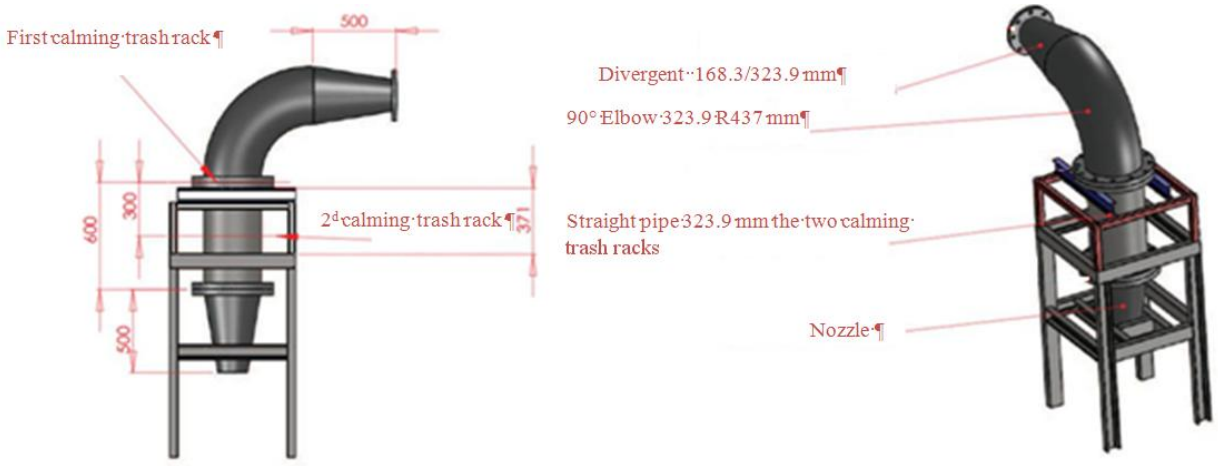

Figure 3: Injector details and detail of the RBI probe

If the void fraction measured by the optical probe was below 0.02, it was assumed that the probe was outside the bubble plume. Hence this criterion enables to determine the Z max which is the penetration depth, and the X max of the bubble plume. As a result, a total of 800 measurement points were recorded during the channel experimental runs.

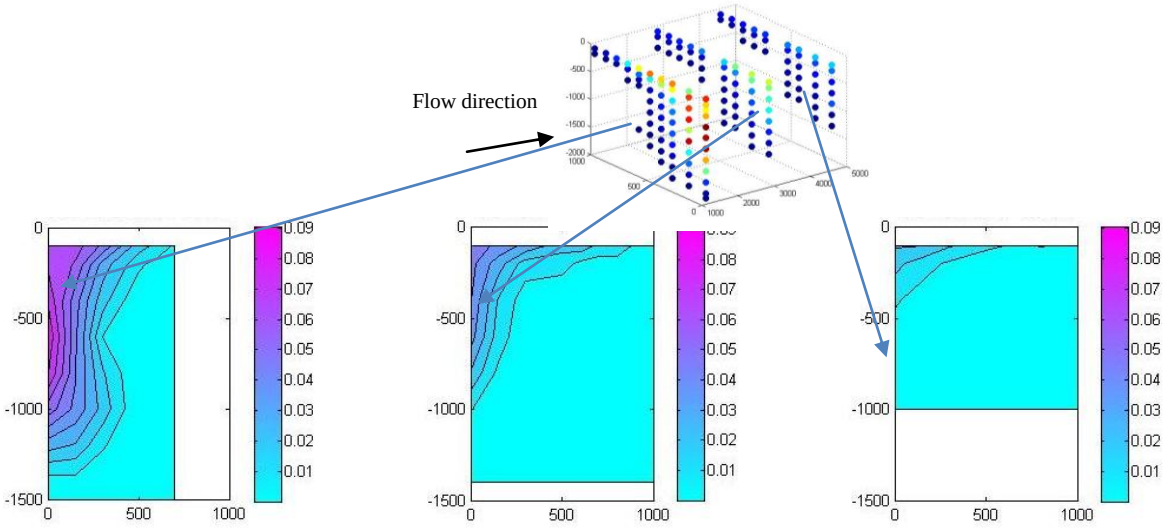

Figure 4: Iso-contours of the void fraction (color scale) over the three half vertical cross-sections located 1, 2.8 and 4.6 m downstream the jet impact location (D_0 135 mm, Q=0.11 m^3s^{-1}).

Basically the optical probe signal provides the indicator function of the phases detected by the probe tip. Hence, the void fraction (α) is simply the total time spent in the gas phase (Tg) divided by the acquisition time (T_t). Void fraction maps over all three sections can then be drawn as shown figure 4.

2.3. Lab Experimental apparatus

The same hydraulic network was erected at the CERG, but in this second experiment the jet fell into a dry channel. The void fraction and the dynamic pressure were measured over 3 jet cross-sections located 0.27 m, 0.94 m and 2.57 m downstream the nozzle outlet (Figure 5). A minimum of 11 measurement points were collected along a jet diameter, the latter was determined by visualization. Around 220 points were collected during these runs.

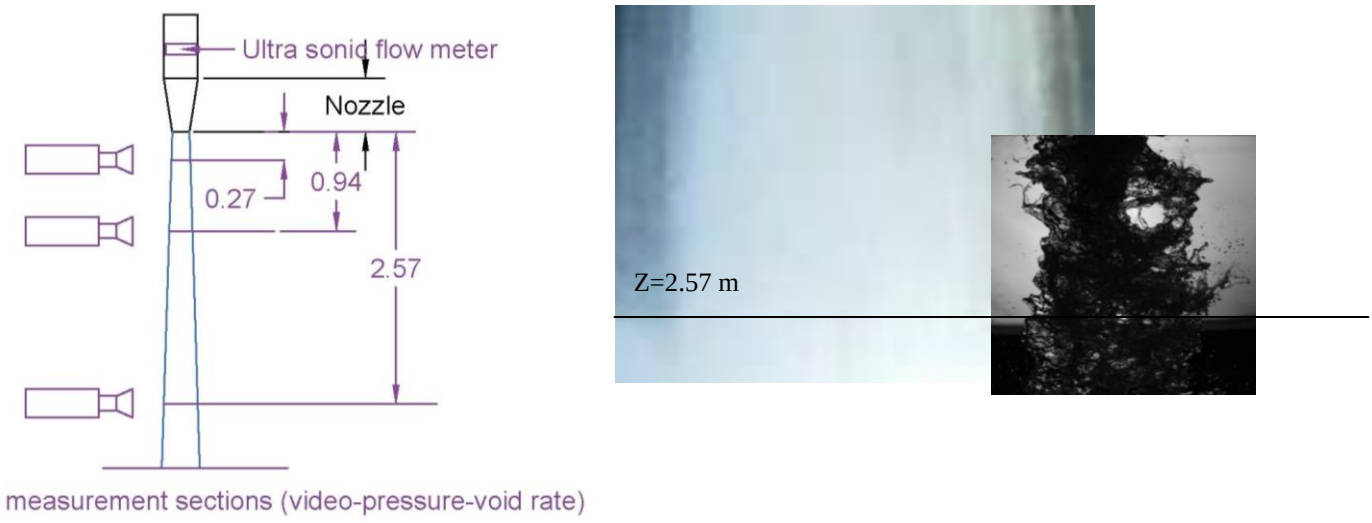

(a) (b) (c)

Figure 5: Scheme of the CERG lab experimental apparatus (a), 24 pictures/s view (b) and high shutter speed picture (c) from the nozzle $D_0$135 mm Q =0.11 m^3s^{-1} z=2.57 m (free surface impact same scale).

The dynamic pressure sensor used is a small FGP sensor XPM5-S126, 10 000 Hz sampling. A minimum of 50 000 pressure values have been recorded for each pressure, representing about 5 seconds run. High speed cameras gave the opportunity to collect movies of the different jets during the laboratory runs. All the high shutter speed movies were performed after the completion of the dynamic pressure and void fraction measurements. Video tools were 2 Phantom Miro M310 cameras (5 040 frames per second for a 896*720 pixels resolution), used with three lenses Nikkon, 60 micro Nikkor, Nikkon 105 micro Nikkor 180 mm APO macro Sigma. The lighting system comprised two alpha 4K 4kW electronic ballast and a Chimera Lighting box.

3. PLUNGING JET AIR ENTRAINMENT

3.1. Bubble size under the free surface

Assuming that the bubble dynamics is not significantly affected by their previous fall, the bubbles are therefore entrained by the horizontal channel velocity after a time scale equals to 1/3 of the diffusion time (τ in s).

$$\tau = \frac{d^2}{\nu} \qquad \textit{(5). Diffusion time}$$

Where d is the bubble diameter (m) and ν the kinematic viscosity (m^2s^{-1}) of the surrounding fluid.

For millimeter size bubbles in water, the order of magnitude of 1/3*τ is 0.3 s. It means that the bubble velocity in the first section located 1 meter downstream the jet impact is already equal to the water velocity (1.35 m s^{-1}). Consequently the "measured bubble diameter" (d,) has been obtained by multiplying the average gas residence time (T_g) detected by the probe by the average channel velocity (V_c) along the horizontal.

$$\boldsymbol{d = T_g * V_c} \qquad \textit{(6): Measured bubble diameter}$$

The average measured bubble diameter for all experimental conditions happens to be comprised between 2.2 and 2.8 mm. It has been found only one literature reference addressing the question of the bubble diameter Simonin (1959). The first attempt to forecast the bubble diameter was based on the equation (4) coupled with the equation (11) which forecast the air entrained flow rate (Figure 6). The second way of predicting bubble size was to calculate the average bubble size using the measured air entrained flow rate in the equation (4). Whatever the way used, the calculation provides a bubble size above 3mm, and thus overestimates the experimental founding. This

shows that the bubble size created by jets similar to the one currently studied is not well predicted even though the order of magnitude is correctly captured.

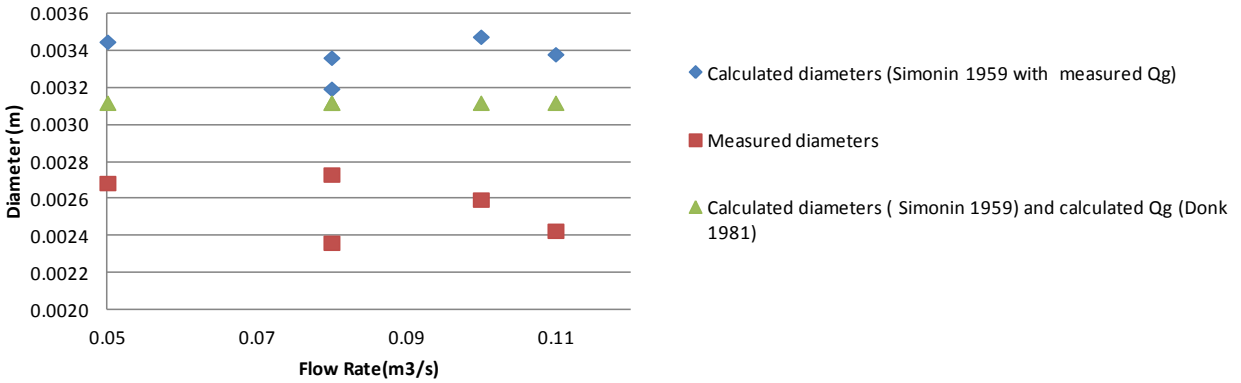

Figure 6: Evaluation of the bubble average diameter

$$d = 4.3*10^{-3}\left(\frac{Q_g}{Q}\right)^{1/3} \qquad \textit{(7) : Average bubble diameter (m) (Simonin)}$$

Where Q_g is the entrained air flow rate and Q is the jet flow rate (m^3s^{-1}).

3.2. Penetration depth

A simple way to border the bubble behavior and evaluate the uncertainty on the penetration depth due to the location of the first measurement section is to analyze the bubble movement.

With the same bubble assumptions as in the previous chapter, the bubble horizontal velocity is equal to V_c. The bubble ascent velocity ranges from 0.2 m/s to 0.3 m/s for Morton numbers between 10^{-13} to 10^{-3}. Hence the ascent slope (ascent velocity/bubble horizontal velocity) range is 0.15 to 0.22. That means that regarding the penetration depth, the maximum approximation is around 20 cm. Thus the measured penetration depth has been directly compared to the calculated ones.

$$M = \frac{g\mu^4\left(\rho_l - \rho_g\right)}{{\rho_l}^2 * \sigma^3} \qquad \textit{(8): Morton number}$$

Where g is gravity acceleration, μ is the liquid dynamic viscosity, ρ_l and ρ_g are the volumetric mass density of the liquid and of the gas, σ is surface tension. all in SI units.

Two main ways have been proposed to predict the penetration depth (H). Some authors have used the continuity or momentum equations Clanet and al.(1997) and Albertson and al.(1950) followed by Falvey and al.(1987) to determine semi empirical equations which provide the penetration depth. Others such as McKeogh and al.(1981), Nakasone (1987) have proposed empirical formulae. The predictions for our flow conditions range from 1 to 10 meters. The experimental measurements happen to be close to the Nakasone results (Figure 7).

$H = 2.6*(V_i D)^{0.7}$	$\frac{V_i}{U_T} = 3.12*\left[\frac{D}{H} + 4*\tan(\alpha)\left(4\frac{H}{D}\right)*\tan^2(\alpha)\right]$	$H = \frac{2}{3}*H_C$	$\frac{H}{D} = \frac{1}{2\tan(\alpha)}\frac{V_i}{U_T}$
(9) McKeogh and al. (1981)	*(10) Falvey and al.(1987)*	*(11) Nakasone, (1987)*	*(12) Clanet and al.(1997)*

Table 2: Penetration depth relations

Where V_i is the jet velocity at impact, U_t is the bubble terminal velocity, D the jet diameter at impact, H the penetration depth and α the jet open angle under the free surface.

The comparison clearly points out the fact that only the Nakasone proposal is close to the current experimental data. The other relations give a wrong order of magnitude.

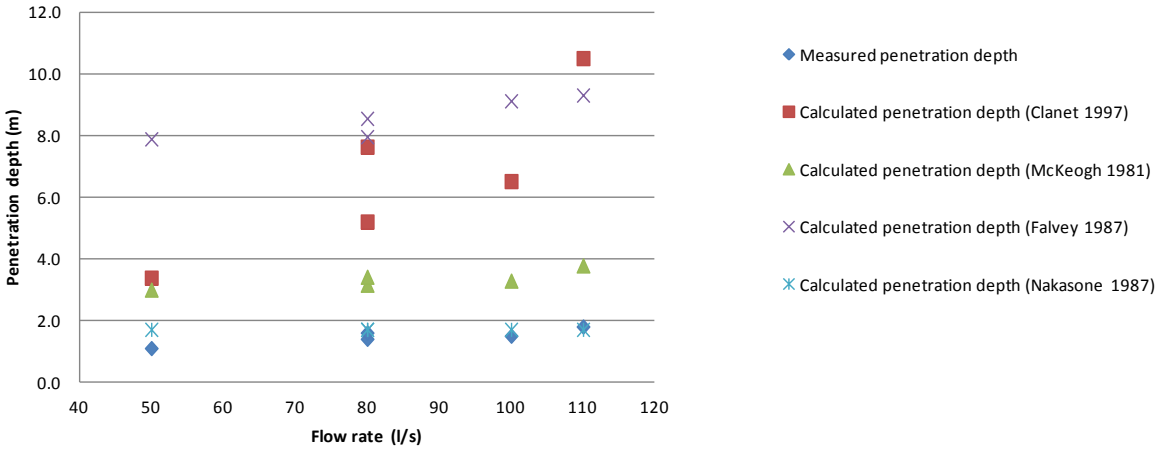

Figure 7: Penetration depth measurement (en X=1m) and literature formulae

3.3. Ascent slope of the bubble plume bottom

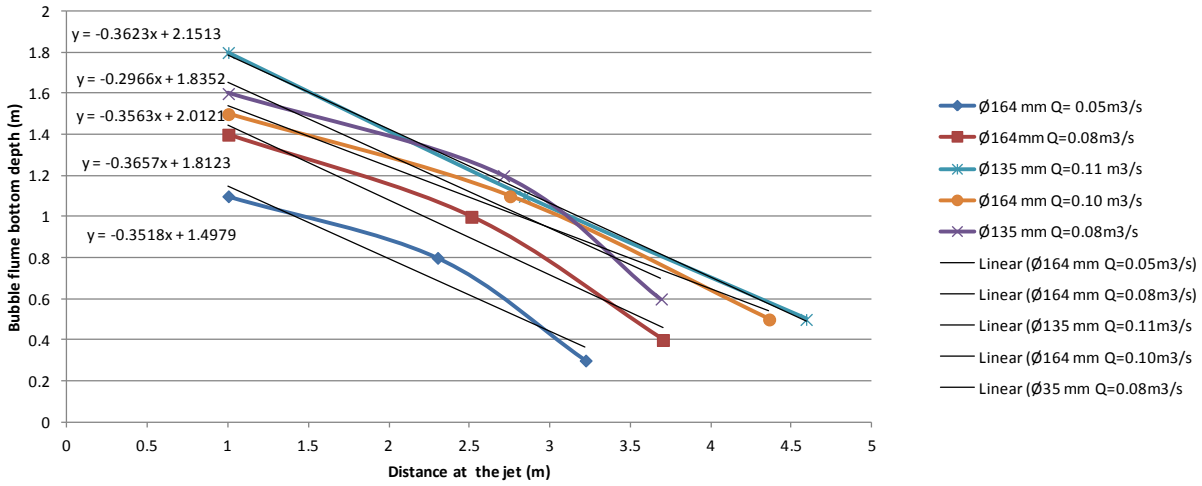

Figure 8: Ascent slope of the bubble plume bottom for all the jet cases

Thanks to the measurements, it is possible to measure the bubble depth in all sections. Hence it is possible to determine the measured ascent slope of the bottom of the bubble plume. The average slope for the 5 cases is equal to 0.35 as shown in Figure 8. If the average channel velocity is the bubble horizontal velocity, the average accent velocity of bubbles would be equal to 0.48 ms^{-1}. Using the Morton number it means that the average bubble diameter would be over 10 mm. These results show without doubt a gap between the classical forecasting relation and the physical behavior of the bubble plume. To conclude, the dynamic ascent of the bubble plume was measured and is strictly different than an isolated bubble velocity ascent.

3.4. Air flow rate entrained (Q_g)

$$Q_g = 1.3*10^{-4}\left(\frac{1}{2}\rho_l * Q * V_i^2\right)^{0.61}$$

(13): Air flow rate entrained by Elsawy and al.(1980)

$$Q_g = 0.09 * Q * \left(\frac{L_c}{D_0} \right)^{0.65} \qquad \textit{(14): Air flow rate entrained by Donk, (1981)}$$

Where L_c (m) is the fall height between the nozzle and the free surface.

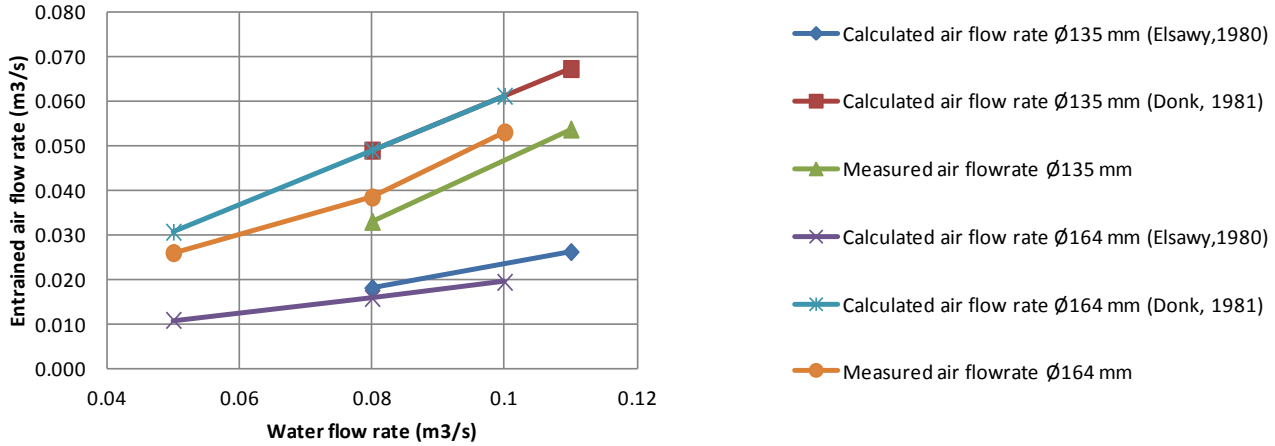

Figure 9: Comparison between measured entrained air flow rate and the calculated one

The two relations have been compared and analyzed in Bin's review paper (1993) on air entrainment. The experimental set ups considered by Bin correspond to jet powers $N_j = 0.5 * \rho_l * Q * V_i^2$ up to 100 W. For the conditions on this study, the jet power is around 10 kW, which is two orders of magnitude larger.

$$F_l = \alpha * V_c \longrightarrow Q_g = \sum_i F_l * S_i \qquad \textit{(15) Calculated entrained air flow rate}$$

Where S_i (m^2) is the influence area of the local flux.

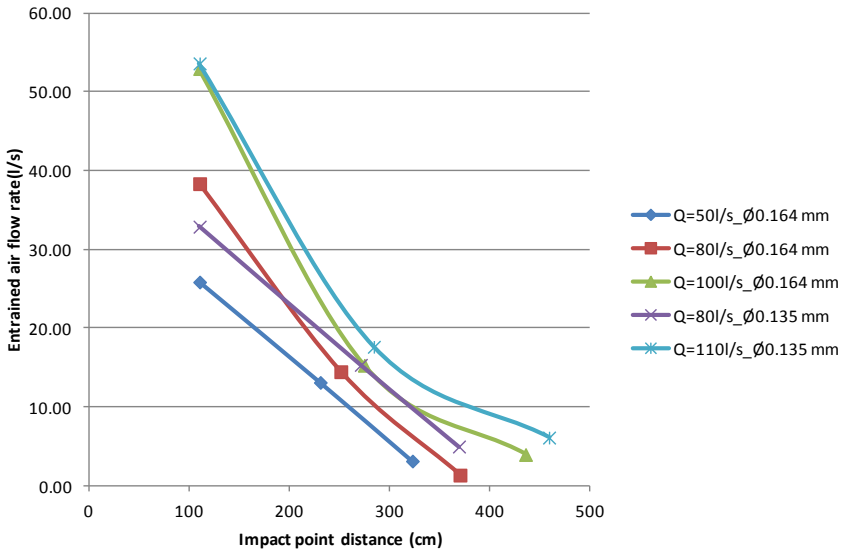

Figure 10: Experimental results for the entrained air flow rate downstream the jet impact point.

A local gas flux (F_l, ms^{-1}) can be calculated as the measured void rate multiplied by the bubble velocity taken equal to the channel velocity. The entrained air flow rate (Q_g) (m^3s^{-1}) is then computed by integrating the local flux over the channel cross-section. Measured air entrained flow rates lie between the two predictions but the interval between the two predictions (Figure 9) evolves with a factor three. In Figure 10 , the measured air flow rate evolution downstream the jet impact has been drawn. In the current cases the ratio (Q_g/Q) is between 40 % and 54 % 1 meter downstream the impact point. This ratio rapidly decreases down to 10 % at 5 m downstream the jet impact location. Evaluating precisely the error linked with the measured air flow rate is tricky. Consequently the comparison results point out the lack of precision on the air entrainment prediction for this kind of jets.

4. JET STATE

The purpose here is to investigate the jet state during the fall and to compare the experimental results with the available literature In particular the calculation of the turbulent intensity (Tu) in the studied jets is needed to compare especially with the Ervine's studies.

4.1. Jet dynamic Pressure

A simplified calculation of the mean dynamic pressure can be achieved assuming a free fall velocity converted into a dynamic pressure into the following chart.

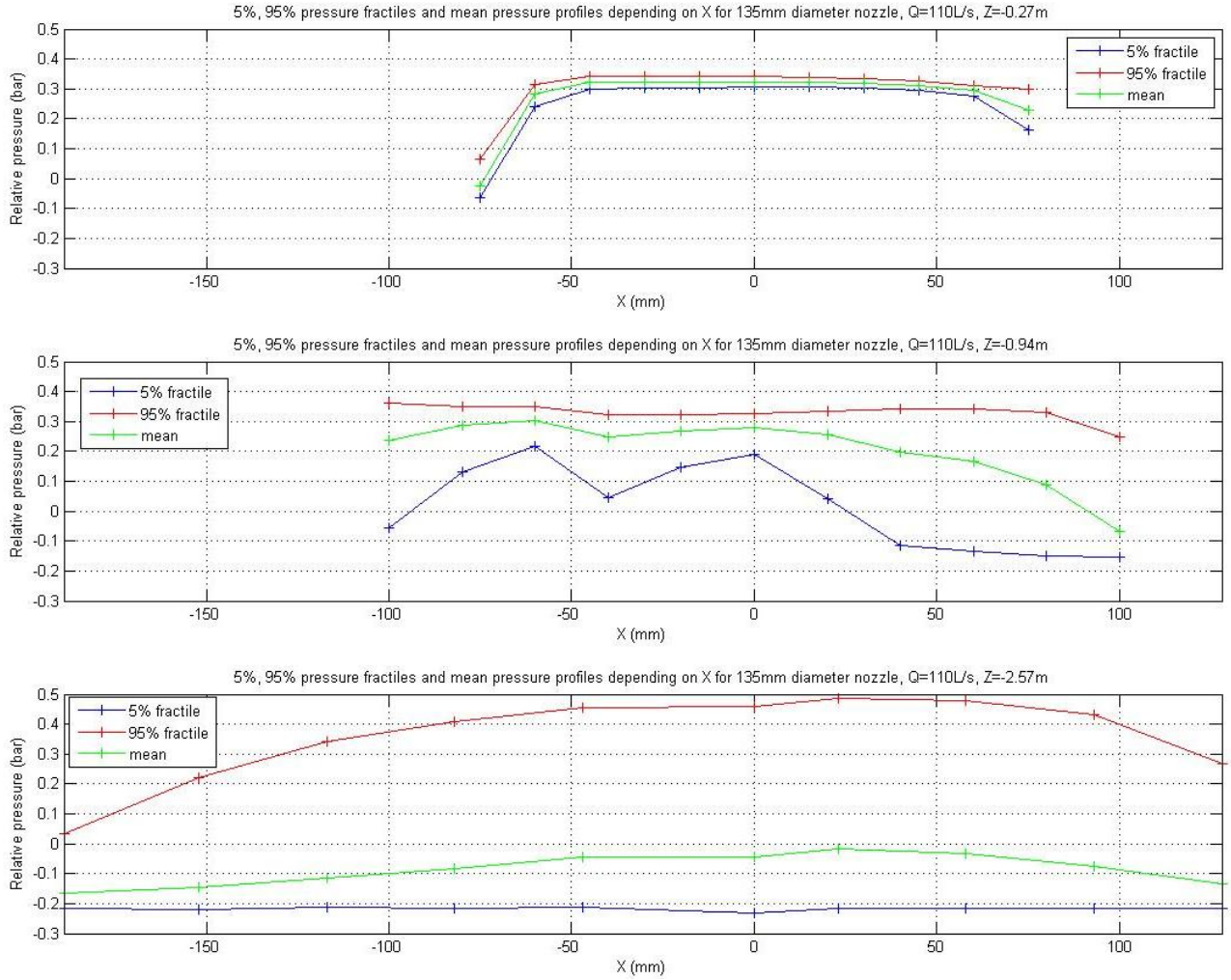

Figure 11: Dynamic pressure across the jet on the three measurement sections under the 135 mm nozzle Q =110 l/s.

Fall height under the Nozzle (L_c) (m)	Calculated dynamic pressure Ø 135mm Q 80L/s (bar)	Calculated dynamic pressure Ø 135mm Q 110L/s (bar)	Calculated dynamic pressure Ø 164mm Q 50L/s (bar)	Calculated dynamic pressure Ø 164mm Q 80L/s (bar)	Calculated dynamic pressure Ø 164mm Q 100L/s (bar)
0	0.153	0.290	0.028	0.071	0.111
0.27	0.179	0.316	0.053	0.098	0.138
0.94	0.245	0.382	0.119	0.163	0.204
2.57	0.405	0.542	0.279	0.323	0.364

Table 3: Simplified calculated dynamic pressure for all the measured sections and cases.

The calculated values are close to the measured jet centered values of the jet for the first two or three sections depending on the case but the last sections values are rather far from the calculated values.

A general trend is that the measured pressures are lower than the calculated ones. It can be concluded that the perturbations linked with surrounding air are directly liable for the acceleration of the jet boundaries.

In addition, the spectral densities of the pressure fluctuations were computed. The spectral density is the Fourier transform applied to discrete fluctuation pressure data. The goal was to understand the jet fluctuations thanks to the dynamic pressure measurement. For all cases, no clear density peak appears on the spectra. The explanation of this unexpected observation may be that the pressure sensor is totally static whereas the jet is flapping as illustrated on the high shutter picture (Figure 5).Consequently this way of measuring cannot provide precisely the jet fluctuations. However it is distinctly observed that the energy (>10^{-5} Bar^2/Hz) is mainly concentrated in the low frequencies (<10^2Hz) structures for all jets.

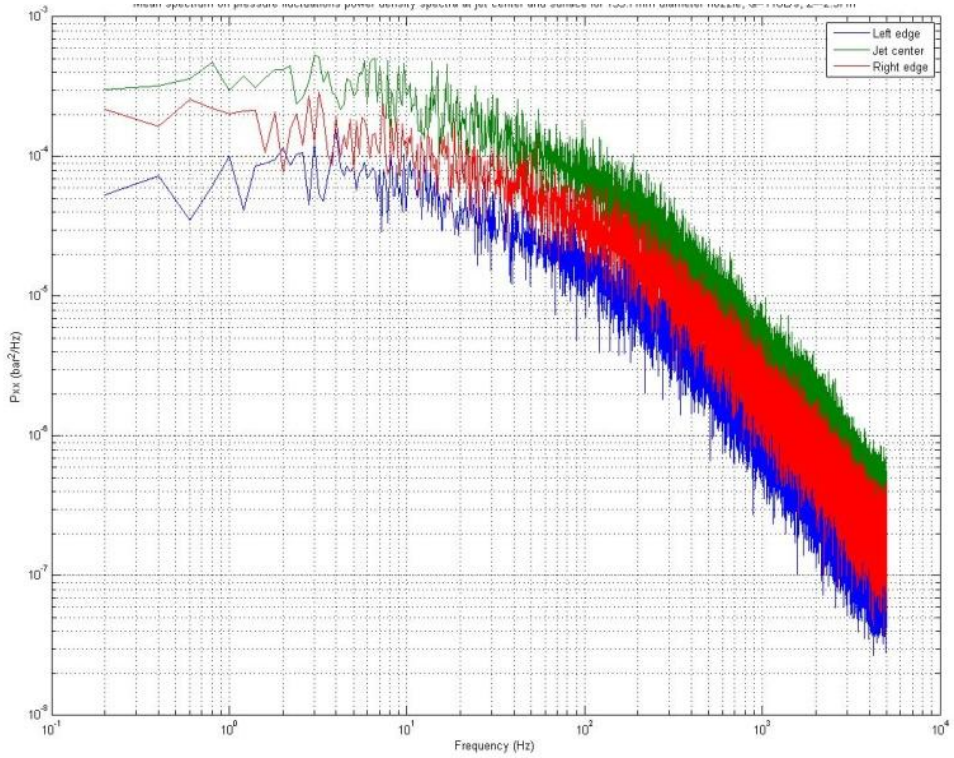

Figure 12: Power spectral density of dynamic pressure fluctuations D_0 135 mm Q= 110 l/s ,z= 2.57 m

4.2. Turbulence intensity (Tu)

D_0 (m)	0.135	0.135	0.164	0.164	0.164
Q (m^3s^{-1})	0.08	0.11	0.05	0.08	0.10
Tu (%)	5	3	20	8	7

Table 4: Tu estimated value for the different cases.

$$Tu = \sqrt{1/n \sum_1^n P_{iT}} \Big/ \sqrt{P_M}$$ *(16): Tu calculation*

Where n is the number of pressure values recorded in one run, P_{iT} is the instantaneous total pressure and Pm is the average pressure (Pa).

The Tu have been estimated with the analysis of the dynamic pressure in the jet cross-section located at z=0.27m. A local Tu has been calculated as described in the previous equation (16) for each measurement point located in the jet (α >0.8). The final Tu is an average of all the local Tu inside the jet. The uncertainty regarding this Tu value is fairly large because of the difficulties in estimating the jet diameter at the section z=0.27m. The 20 % uncertainty value given for the 164 mm diameter and 0.05 m3/s flow rate is due to this reason. In this case the jet fluctuations began before the 0.27m section. The experimental set up was not well adapted to this relevant parameter because the pressure sensor is totally static whereas the jet center in the corresponding section is moving.

4.3. Void rate

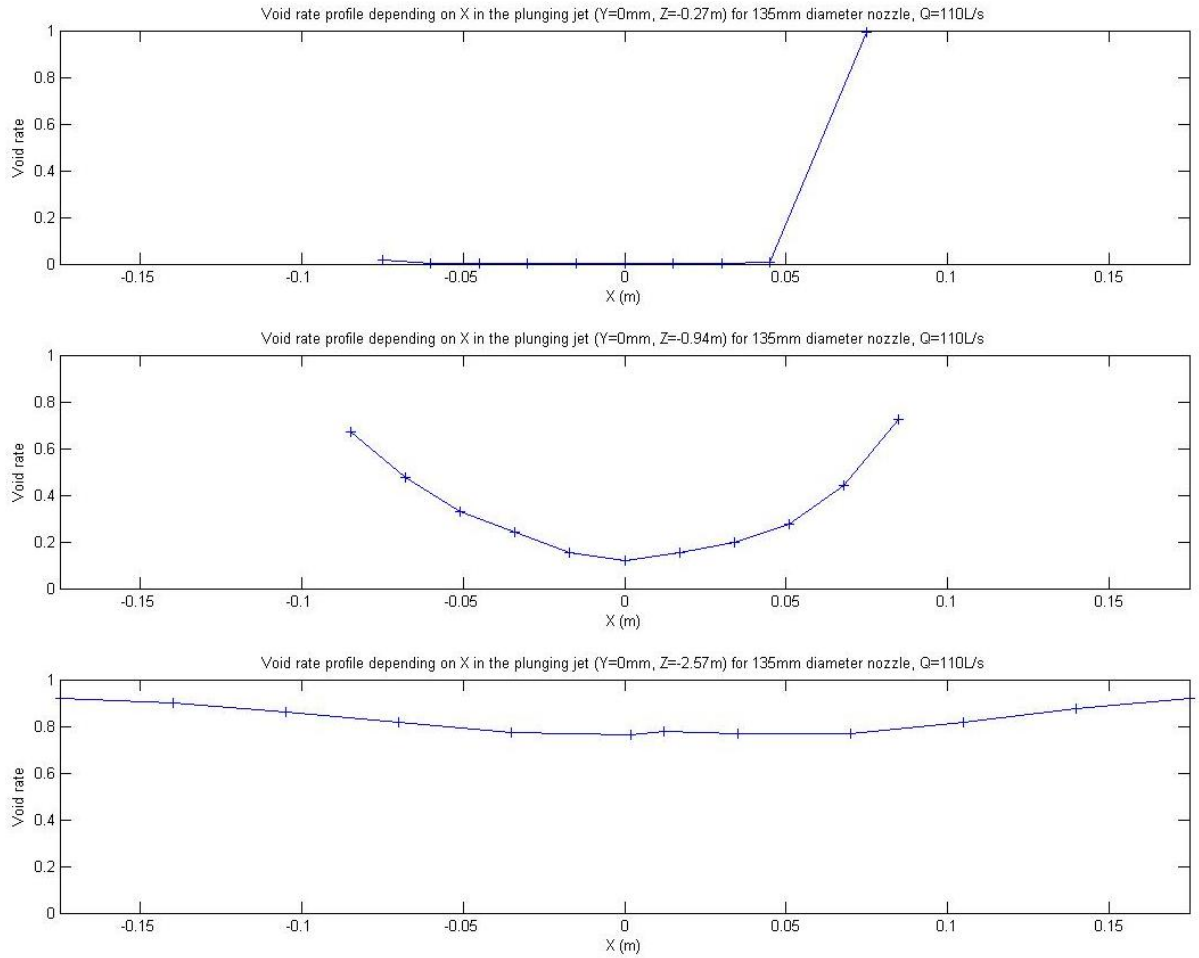

Figure 13: Void fraction profiles across the jet at different distances from the nozzle (D_0 135mm, Q =110 l/s)

For all the cases the void rate in the first measurement section is definitely equal to zero indicating that the ambient air hasn't yet disturbed the jet. The point where the void rate is equal to one shows that the probe was located at the border of the jet.

For the other sections, the air penetration is well defined by the measurements. Especially at the 2.57 m section, the over 80% void fraction value may indicate that the jet is atomized. Again, the problem is that the probe was static in a fluctuant jet that induces the same consequences as for pressure measurement. The void fraction is close to 1 all over the last section (2.57 m). Accordingly it may easily be extrapolated that the jet is atomized.

4.4. Break up Length

The fall length where the jet becomes a discontinuous structure is usually called the break up length. Different formulae to predict the break up length have been proposed (Bin, 1993):

$\frac{L_b}{D_0} = \frac{1.05}{1.14 * Tu}$	$L_b = 6 * Q^{0.32}$	$L_b = C * Q^s$
(17) Ervine and al., 1997	*(18) Horeni (1956) quoted in Le Castillo, (2007)*	*(19) Elsawy and al., (1980)*

Table 5: Break up length relations compared with the experimental data

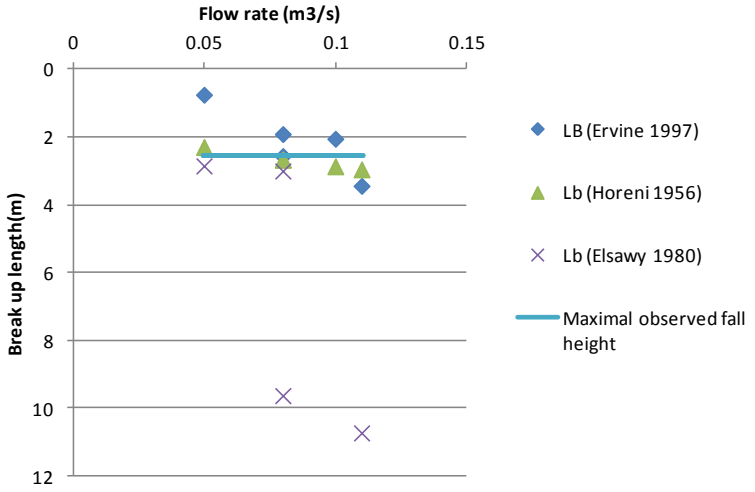

Figure 14 : Comparison between the different literature breaking lengths

Where, Tu is the turbulent intensity, Lb the break up length and C and S are empirical coefficients related with the turbulence intensity. To exploit Ervine et al. proposal, we considered two reasonable values for Tu, close to what is expected in a fully developed pipe flow, namely Tu=3% for Ø135 mm and Tu= 8% for Ø164mm. This comparison coupled with the jet void rate and dynamic pressure before the impact suggests that for 3 cases out of 5 the jet is atomized or nearly atomized

On the contrary, the high shutter speed videos have proved that none of the jets. The shutter speed pictures prove that the jet undulations are significant. Thus coupled with the human view it leads to a misunderstanding of the jet structure during the fall. In a nutshell, the jet flapping is the explanation of the large void fraction and the pressure fluctuations measured with the other ways of measurement.

We have studied is atomized for a 2.57 m falling length. As a conclusion, the classical relations seem to be inapplicable to the jets considered in these experiments. The videos show that while other results suggested an atomized jet, the jet is actually not atomized, but destabilized during its fall (Figure 5).

5. CONCLUSION

Five large jets, large with respect to the nozzle diameter, the flow rate and the fall height flow rate, were tested during this study. The bibliography has proved to be particularly poor concerning the air entrainment consequences of such the large plunging jets. The main unknown variables such as the bubble diameter, the penetration depth, the bubble plume bottom ascent velocity and the entrained air flow rate have been measured and compared to the main relationships available in the literature. It has incontestably been pinpointed that the case of large scale jets is still not well understood and their consequences in terms of air entrainment still escape prediction. The jet structure before the impact is probably the key point to forecast the jet consequences in terms of bubble generation. That is

the reason why the second step of runs has been achieved. It has been underlined that conventional methods coupled with the human vision leads to a misunderstanding mainly because of the jet flapping motion. Therefore only the high frequency imaging enables to correctly analyze the motion and the real behavior of the jet during its fall. The conclusion is that it is still necessary to find the correct parameters that govern the evolution of a large jet from the nozzle to the plunge pool. To reach this purpose a large scale experiment should be carried out to relate the bibliographic results concerning the small and medium scales with large scale jets situations.

6. ACKNOWLEDGMENTS

The authors are deeply grateful to IRIS (Grenoble-INP) especially François BONNEL for his strong support with the high shutter speed films.

The laboratory LEGI is part of the LabEx Tec 21(Investissements d'Avenir-Grant Agreement No. ANR-11-LABX-0030).

7. REFERENCES

Albertson, M.L., Dai, Y.B., Jensen, R.A., Rouse, H., (1950), Diffusion of Submerged Jets. American Society of Civil Engineers, Vol. 115, No. 1, January 1950, pp. 639-664

Bińi, A.K., (1993). Gas entrainment by plunging liquid jets. Chemical Engineering Science 48, 3585–3630.

Castillo, L.G., (2007). Pressures Characterization of Undeveloped and Developed Jets in Shallow and Deep Pool, IAHR World congress, Venise.

Clanet, C., Lasheras, J.C., (1997). Depth of penetration of bubbles entrained by a plunging water jet. Physics of Fluids 9, 1864.

Donk, J. van de, (1981). Water aeration with plunging jets. Dutch Efficiency Bureau, Pijnacker.

Duarte, R.X., (2014). Influence of Air Entrainment on Rock Scour Development and Block Stability in Plunge Pools. EPFL, Lausanne.

Elsawy, E., Mckeogh, E., Ervine, D., (1980). Effert of turbulence intensity on the rate of air entrainment by plunging water jets. ICE Proceedings 69, 425–445

Ervine, D.A., Falvey, H.T., Withers, W., (1997). Pressure fluctuations on plunge pool floors. Journal of Hydraulic Research 35, 257–279.

Evans, G.M., Jameson, G.J., Atkinson, B.W., (1992). Prediction of the bubble size generated by a plunging liquid jet bubble column. Chemical Engineering Science 47, 3265–3272.

Falvey, H., Ervine, D., (1987). Behaviour of turbulent water jets in the atmosphere and in plunge pools, ICE Proceedings 83, 295–314.

McKeogh, E.J., Ervine, D.A., (1981). Air entrainment rate and diffusion pattern of plunging liquid jets. Chemical Engineering Science 36, 1161–1172.

Nakasone, H., (1987). Study of Aeration at Weirs and Cascades. Journal of Environmental Engineering 113, 64–81.

Simonin RF, (1959). Recherches théoretiques et expérimentales sur l'entrainement d'air par une veine d'eau cylindrique percutant dans une masse d'eau. Presented at the 8th Congress of IAHR, AIRH, Montreal.